Modeling of optical aberrations due to thermal deformation using finite element analysis and ray-tracing

Tobias Bonhoff*[a], Lasse Büsing[a], Jochen Stollenwerk[a,b], and Peter Loosen[a,b]
[a]Chair for Technology of Optical Systems, RWTH Aachen University,
Steinbachstr. 15, 52074 Aachen, Germany;
[b]Fraunhofer Institute for Laser Technology, Steinbachstr. 15, 52074 Aachen, Germany

ABSTRACT

Thermo-optical simulation is an important extension of classical ray-tracing because many applications, especially in laser technology, have to deal with thermal effects. This paper discusses an approach for modeling thermally induced surface deformations of rotational symmetric optical systems: the discrete deformation data generated by Finite Element Analysis (FEA) are approximated using a global even polynomial which is then transferred to the ray-tracing. The implemented algorithm is validated by comparing approximated data to an analytic deformation function. Finally, the benefit of modeling the temperature dependent refractive index and the thermal deformation is demonstrated using the example of a plastic lens.

Keywords: Thermal deformation, optical surface deformation, finite element analysis, ray-tracing, thermal lensing, opto-mechanical analysis

1. INTRODUCTION

Thermal lensing in optical systems for laser beam guiding and shaping can lead to a significant focal shift and a degradation of the focal intensity distribution. Especially when utilizing multi-kW lasers with high brilliance, thermal effects have to be taken into account to achieve a stable process. Moreover, the imaging quality of coaxial process monitoring might be diminished by thermally induced aberrations [1]. For plastic optics, thermal effects already occur at low power because compared to optical glasses, the absorption coefficient and thermal expansion are high.

Absorption of laser energy by the bulk material and the coating leads to an inhomogeneous heating of the optical components and causes a locally varying refractive index. In addition, surface deformations and thickness variations due to thermal expansion influence the optical behavior. In order to compensate these thermo-optical effects, a precise modeling is required. Since commercially available ray-tracing software such as ZEMAX® [2] cannot handle inhomogeneous temperature variations, it is reasonable to combine the advantages of Finite Element Analysis (FEA) and ray-tracing.

Different approaches for coupling FEA and ray-tracing have been realized over the last years [3–6]. At our Chair, an interface between FEA and ZEMAX® has been developed which enables a precise modeling of the temperature dependent refractive index profile, even at high field angles, and the optimization of thermally aberrated systems [7–9]. The discrete temperature data from FEA are approximated using an adaptive weighted least squares method.

To take full advantage of this coupling, we extended it in order to model the thermally induced surface deformation and change in thickness of optical elements. In contrast to other approaches that utilize Zernike polynomials to model the surface deformation [4,10–12], we use a global even polynomial. It has been shown that for optical systems featuring rotational symmetry, the approximation of a global polynomial is fast and accurate. Section 2 discusses the pre-processing of FEA data, the approximation, and the implementation into the optical ray-tracing. In section 3, the presented algorithm is verified and finally applied onto an example in section 4.

2. MODELING OF THERMAL DEFORMATION

Ray-tracing in Zemax® requires that each optical surface is defined as a sag. The sag is the distance of the optical surface from its vertex measured parallel to the optical axis. Furthermore, the surface sag has to be a continuously differentiable function since the surface normals are needed to compute the refraction. But the FEA usually provides only discrete deformation data for the nodes, either in Cartesian or cylindrical coordinates. Thus, three steps are

*tobias.bonhoff@tos.rwth-aachen.de; phone +49 241 8906 379; fax +49 241 8906 121

necessary to transfer the thermal deformation to Zemax®. Firstly, in a pre-processing step, the deformation data from the FEA are mapped onto the optical axis to receive the effective axial deformation, in the following called deformation sag. Secondly, the discrete deformation data are approximated into a continuously differentiable function. Finally, this function is added as an additional sag to the original surface sag in Zemax® via a user defined surface. These steps are described in more detail in the following paragraphs (2.2–2.4).

2.1 Example for axial and radial deformation

Lenses do not only expand in axial direction when they heat up but also in radial direction. For curved surfaces, the contribution of radial deformation is normally not negligible. The thermal deformation of a common biconvex lens made of N-BK7 serves as an example. In the simulation, the curvature radii are assumed to be ±50 mm and the diameter 25.4 mm. The beam features a top-hat shape and a diameter half as large as the lens diameter. Further parameters can be found in table 1. The temperature at the lens edge is fixed to 22°C. It is assumed that the lens is clamped at its edge so that it cannot expand in radial direction. The FEA in Ansys® [13] predicts a temperature increase up to 74°C at 500 W optical power which leads to a maximal axial deformation of 163 µm while the maximal radial deformation is 111 µm (cf. figure 1). The ratio of radial and axial deformation depends on the geometrical shape of the lens, the beam profile, the clamping, the cooling conditions, and other parameters. However, a precise optical modeling requires taking into account the radial deformation.

Table 1. Material parameters for N-BK7 [14] and lens parameters used in the FEA.

Parameters for N-BK7	Value	Lens parameters	Value
Thermal conductivity [W/m·K]	1.114	Diameter [mm]	25.4
Thermal expansion coefficient [1/K]	$8.3 \cdot 10^{-6}$	Curvature radii [mm]	+50 / −50
Absorption coefficient [%/cm]	0.12	Center thickness [mm]	5.0
		Optical input power [W]	500
		Edge temperature [°C]	22

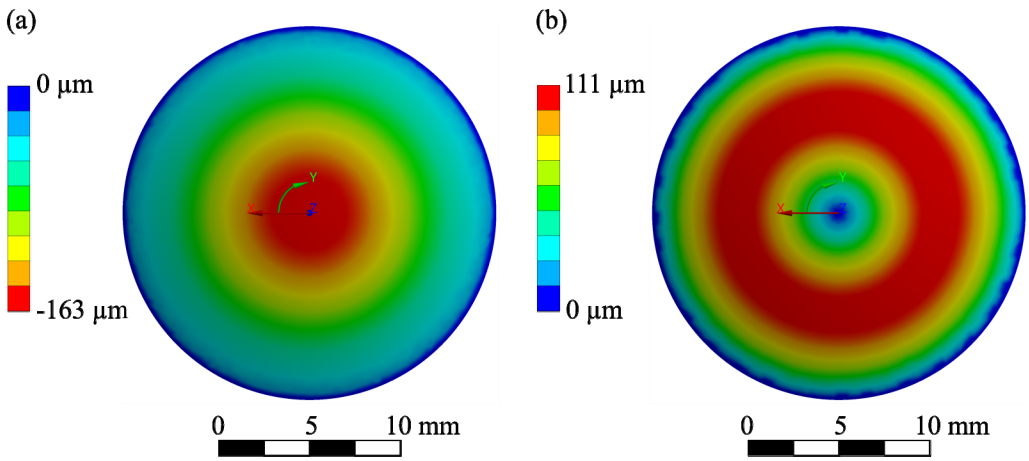

Figure 1. Comparison of the axial (a) and radial deformation (b) of a biconvex lens with 50 mm curvature radius. The maximal axial deformation is computed to 163 µm while the maximal radial deformation is 111 µm.

2.2 Computing the deformation sag

In order to compute the deformation sag, the shape of the original surface sag is needed. For spherical, conical, and aspherical surfaces, an analytical expression of the original sag is given by

$$z(r) = \frac{cr^2}{1+\sqrt{1-(1+k)c^2r^2}} + \sum_{i=1}^{8} \alpha_i r^{2i}. \tag{1}$$

The curvature of the lens c is the inverse radius R and the conical constant is k. The sum in equation (1) describes the even aspheric terms with the coefficients α_i. Due to thermal deformation, each FE node moves $\Delta r = \sqrt{\Delta x^2 + \Delta y^2}$ in radial direction and Δz in axial direction. The node depicted in figure 2 is displaced from $\mathrm{P}_0 = (r, z)$ to $\mathrm{P}_1 = (r + \Delta r,\ z + \Delta z)$. Analogously, a virtual node can be introduced which is purely displaced parallel to the optical axis from $\mathrm{P}_0^* = (r + \Delta r,\ z - \Delta z_{sag})$ to P_1. The distance from P_0^* to P_1 equals the effective axial deformation, and therefore the deformation sag, and is calculated using the algorithm presented in [11]

$$\Delta z_{eff}(\tilde{r}) = \Delta z + \Delta z_{sag} = \Delta z + \{z(r) - z(\tilde{r})\}, \tag{2}$$

where $\tilde{r} = r + \Delta r$. In equation (2), the terms in curly brackets are computed using the surface sag given in (1). The additional axial distance Δz_{sag} is indicated in figure 2. An advantage of this algorithm compared to others is that the absolute z-coordinates of the nodes are not used so that small inaccuracies of the FE node positions are less important [11].

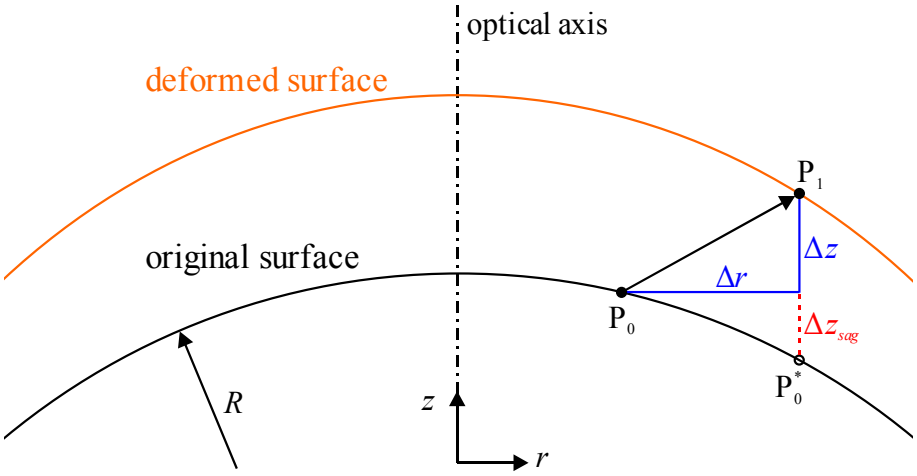

Figure 2. The FE node is displaced from P_0 to P_1 due to thermal deformation. This corresponds to a pure axial deformation of a virtual node from P_0^* to P_1.

2.3 Approximation of the deformation sag

Many optical systems for laser beam guiding and shaping such as beam expanders feature a rotational symmetric optical design. In case of a rotational symmetric beam profile, axial radiation will induce a rotational symmetric thermal load. Hence, the surface deformation will be rotational symmetric, too, and the approximation of a global even polynomial is sufficient to transform the discrete data into a continuously differentiable function. The even polynomial for the deformation sag is given by

$$\Delta z_{eff}(r) = \sum_{j=0}^{p} \alpha_j^{th} r^{2j}. \tag{3}$$

The coefficients α_j^{th} start at order zero, which describes the thickness variation of the optical element. The maximal polynomial degree p may vary between 2 and 16. In most cases, $p = 8$ yields an accurate approximation. For computing the coefficients in (3), a polynomial regression based on weighted least squares methods is used. An advantage of this algorithm is that scattered, i.e. non-equidistant, input data can be handled.

2.4 User defined surface in Zemax®

The approximated even polynomial in equation (3) is added as an additional sag to the standard sag utilizing a user defined surface in Zemax®. The new surface sag is given by

$$z(r) = \frac{cr^2}{1+\sqrt{1-(1+k)c^2r^2}} + \sum_{i=1}^{8} \alpha_i r^{2i} + \sum_{j=0}^{p} \alpha_j^{th} r^{2j}. \tag{4}$$

In addition, the gradient-index lens caused by an inhomogeneous temperature distribution in the bulk is modeled within the user defined surface. More details can be found in [7–9]. Via the coupled simulation, the change in optical behavior, especially the focal shift and higher order aberrations, can be analyzed.

3. VERIFICATION OF APPROXIMATION

In order to verify the correctness of the approximation and the user defined surface in Zemax®, a test case is developed. A plane plate featuring an aspheric deformation (only on the front surface) is assumed. The un-deformed plate is 5 mm thick, 20 mm in diameter and has a refractive index $n = 1.5$. The used even aspheric coefficients are listed in table 1 and correspond to a maximal deformation on the optical axis of 1 mm in negative direction and zero deformation at the lens edge. The original and the deformed surface sag are depicted in figure 3. Based on the analytical expression for the deformation given by equation (3), discrete data are generated with a different number of sampling points $N = 20$, 50, 100, 200, 500, 1000. These discrete data, which are equally spaced in r, are then approximated using the algorithm presented in paragraph 2.3. The maximal polynomial degree p is varied from 4 to 16. The resulting back focal length f of the deformed plate is calculated via an optimization in Zemax® and compared to the expected back focal length $f_{\text{theo}} = 143.169$ mm which is obtained by adding the coefficients to an even asphere. The beam diameter is always 10 mm.

Since real input data resulting from an FEA contain noise, the test case is extended to analyze the influence of noisy input data onto the approximation. A random noise signal $\varepsilon(r)$ is added to the data and the approximation is repeated according to:

$$\Delta z_{eff}^{*}(r) = \varepsilon(r) \cdot \Delta z_{eff}(r), \quad -\varepsilon_0 \le \varepsilon(r) \le \varepsilon_0. \tag{5}$$

Two different noise levels $\varepsilon_0 = 1\%$, 2% are examined. In order to obtain a reliable statistics, for each level, 50 different sets of random noise $\varepsilon(r)$ are added to the data. The average and the root mean squared error (RMSE) of the resulting back focal lengths are calculated for each noise level.

Table 2. Aspheric coefficients used in the test case. The maximal deformation of 1 mm in negative direction occurs on the optical axis while the lens edge is not displaced.

Coefficient	Value
α_0	−1.0
α_2	$6.0 \cdot 10^{-3}$
α_4	$2.0 \cdot 10^{-5}$
α_6	$1.0 \cdot 10^{-7}$
α_8	$1.0 \cdot 10^{-9}$
$\alpha_{10} - \alpha_{16}$	0.0

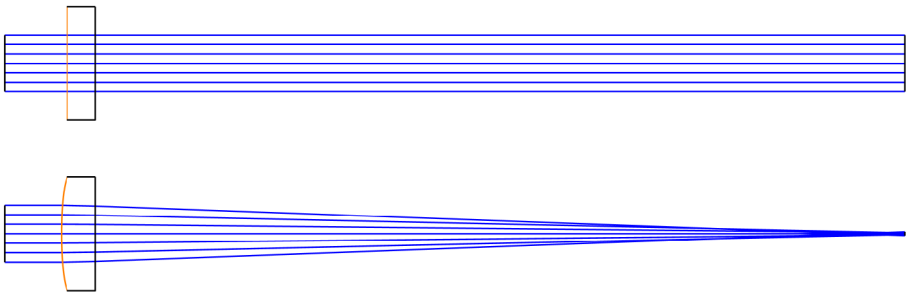

Figure 3. Sketch of the test case. The deformed front surface (bottom) leads to a back focal length of 143.169 mm while the rays pass the un-deformed plate (top) without refraction.

3.1 Influence of the polynomial degree and the sampling

For a fixed number of sampling points $N = 100$, the influence of the maximal polynomial degree p is analyzed. Figure 4(a) depicts the relative focal deviation Δf between f and f_{theo}. For $p = 4$, the focal deviation is in the range of 4–6% since the model does not represent the data. In case of data without noise and $p \geq 8$, the approximated coefficients α_j^{th} almost equal those listed in table 2. The resulting absolute focal deviation is smaller than $4 \cdot 10^{-8}$ mm, which corresponds to a relative deviation of less than $3 \cdot 10^{-10}$. Such small errors are expectable because the input data are polynomial with degree 8 and thus can be exactly described by the model.

In contrast, noisy input data lead to longer focal lengths compared to noise free data. This means the influence of the thermal deformation on the optical behavior is slightly underestimated. For $p = 10$, the smallest mean deviation can be observed: $\Delta f = 0.58\%$ for $\varepsilon_0 = 1\%$ and $\Delta f = 1.3\%$ for $\varepsilon_0 = 2\%$. The smallest RMSE occurs for $p = 4$. Higher polynomial degrees may lead to oscillations of the approximated polynomial and induce higher fluctuations of the focal length.

The number of sampling points N is varied at a fixed polynomial degree $p = 8$ (cf. figure 4(b)), which is the best compromise between a small focal deviation and a small RMSE. For data without noise, 20 sampling points already yield an accurate result. The relative focal deviation is less than $2 \cdot 10^{-11}$. In case of noisy data and $N = 20$, the RMSE of the focal deviation is comparably large. The RMSE clearly decreases with increasing N. When taking the RMSE into account, $\Delta f < 2\%$ is observed for $N \geq 50$ in case of $\varepsilon_0 = 1\%$ and for $N \geq 500$ in case of $\varepsilon_0 = 2\%$. This indicates that a higher sampling rate will reduce the focal deviation for noisy input data.

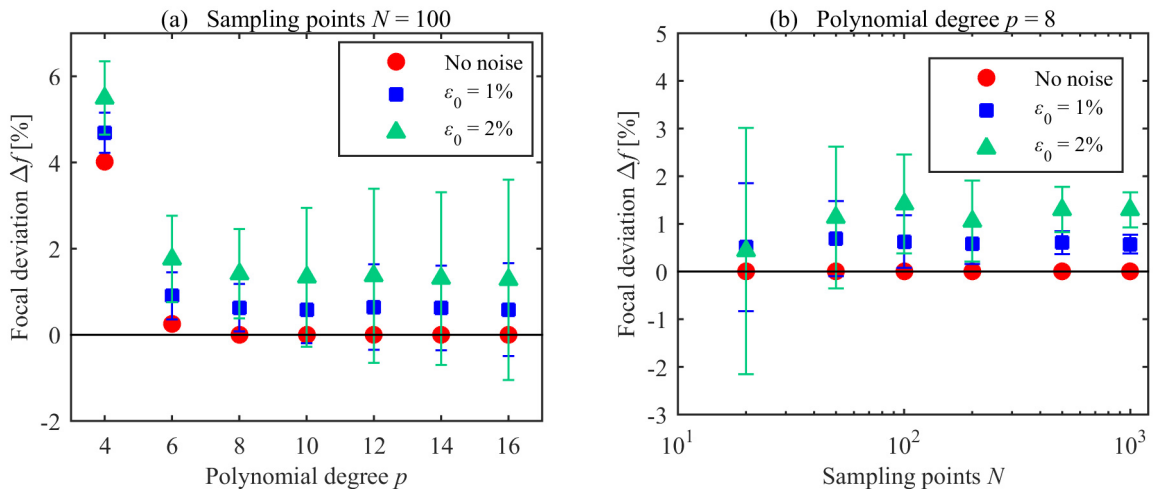

Figure 4. Relative focal deviation plotted (a) versus the used polynomial degree and (b) versus the number of sampling points. In (a), the sampling is fixed to $N = 100$ and in (b), the polynomial degree is set to 8.

3.2 Correlation of RMSE and focal deviation

As the data in figure 5 show, the focal deviation correlates with the RMSE of the approximation (which has to be distinguished from the RMSE caused by 50 sets of random noise in paragraph 3.1). For this analysis, the polynomial degree is fixed to 8 and the maximal sampling $N = 1000$ is used. The RMSE of the approximation scales linearly with the noise level as it increases from 3.8 µm at $\varepsilon_0 = 1\%$ to 7.8 µm at $\varepsilon_0 = 2\%$. For a certain noise level, the resulting relative focal deviation scatters clearly, but still a correlation to the RMSE is evident. Thus, the RMSE is a suitable indicator for the quality of the ray-tracing within Zemax®.

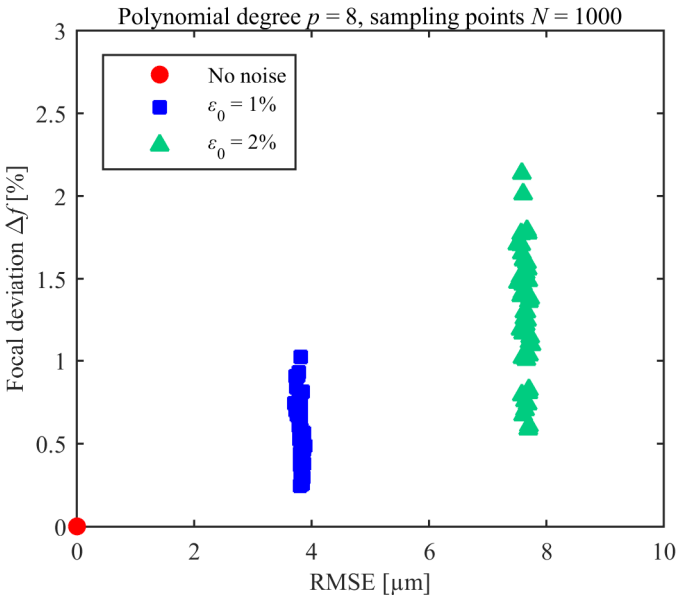

Figure 5. Relative focal deviation plotted versus the RMSE of the approximation. The polynomial degree is fixed to 8 and the sampling points to 1000.

In conclusion, the approximation of a global even polynomial is appropriate for modeling thermally induced surface deformations. Noisy input data lead to reliable results for the focal length because the relative focal deviation is smaller than 1.5% for random noise of 1%. Accordingly, the influence of noise is negligible compared to other disturbing factors such as uncertainties in absorption values, especially for the coating, and in setting up a realistic FEA including the clamping and cooling of optics.

4. EXAMPLE PLASTIC LENS

In order to demonstrate the benefit of modeling the temperature dependent refractive index and the thermal deformation, the thermo-optical behavior of an aspheric plastic lens is analyzed. Compared to optical glasses, plastic features an approximately 100 times larger thermal expansion and thermo-optic coefficient. Thus, thermal effects already occur at low power applications. The silicone elastomer Silopren LSR7070 [15] is chosen as lens material because it features high transparency, is heat-resistant up to 200°C, can be injection-molded and is therefore used in lighting applications [16]. The effective focal length (EFFL) of the asphere is 15.0 mm. The conical constant of the front surface has been optimized to obtain a diffraction limited focal spot. The beam is 4 mm in diameter and features a top-hat shape. Further parameters can be found in table 3. A cross section of the lens and a spot diagram, both for the "cold" system, are shown in figure 6.

The thermo-mechanical analysis is performed with Ansys®. The simulation is limited to a quarter section of the lens in order to reduce the number of nodes. The mesh is tetrahedral and features approximately 40000 nodes. The temperature at the lens edge is fixed to 22°C. It is assumed that the lens is clamped at its edge so that it cannot expand in radial direction. The resulting temperature profile and surface deformation at 5 W optical power are presented in the following paragraphs. The wavelength used in the simulation is 589 nm because for other wavelengths, no data is available for the thermo-optic coefficient.

Table 3. Material parameters for Silopren LSR7070 [15–17] and lens parameters.

Parameters for LSR7070	Value	Lens parameters	Value
Thermal conductivity [W/m·K]	0.19	Diameter [mm]	6.0
Thermal expansion coefficient [1/K]	$2.7 \cdot 10^{-4}$	Curvature radii [mm]	5.5 / 40.0
Thermo-optic coefficient* [1/K] @ 589 nm	$-3.0 \cdot 10^{-4}$	Conical constant	−0.523 / 0.0
		Center thickness [mm]	4.0
Refractive index @ 589 nm	1.4122	EFFL [mm]	15.0
Absorption coefficient** [%/cm]	0.44	Optical input power [W]	5.0
		Edge temperature [°C]	22

* linearly interpolated between values for 25°C and 125°C given in [16]
** calculated based on 53% transmission at 1 m thickness [17] and 2.9% Fresnel reflection per surface

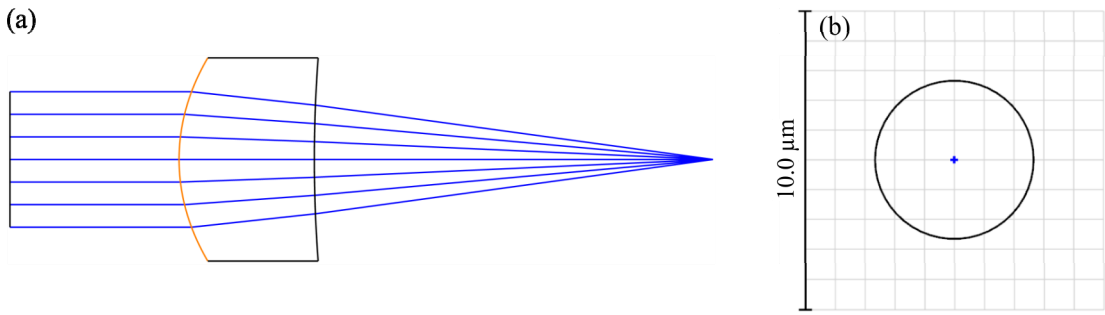

Figure 6. Cross section of the plastic asphere (a) and spot diagram in the focal plane at 589 nm wavelength (b). The circle indicates the Airy disk with 2.7µm radius. The spot size is diffraction limited.

4.1 Modeling of the gradient index profile

In a first step, only the temperature dependent refractive index is taken into account. The temperature profile resulting from the FEA is depicted in figure 7(a). The maximum temperature increase is 1.98°C and occurs on the optical axis. The resulting gradient index profile (GRIN) leads to a clear focus shift of +132 µm. Since the thermo-optic coefficient for LSR 7070 is negative, the focus is shifted to longer distances. The spot size in the original focal plane is no longer diffraction limited because the RMS spot increases to 12.3 µm (cf. figure 7(b) and table 4) while the Airy radius is 2.7 µm. As depicted in figure 7(c), the spot size in the new focal plane is below the diffraction limit.

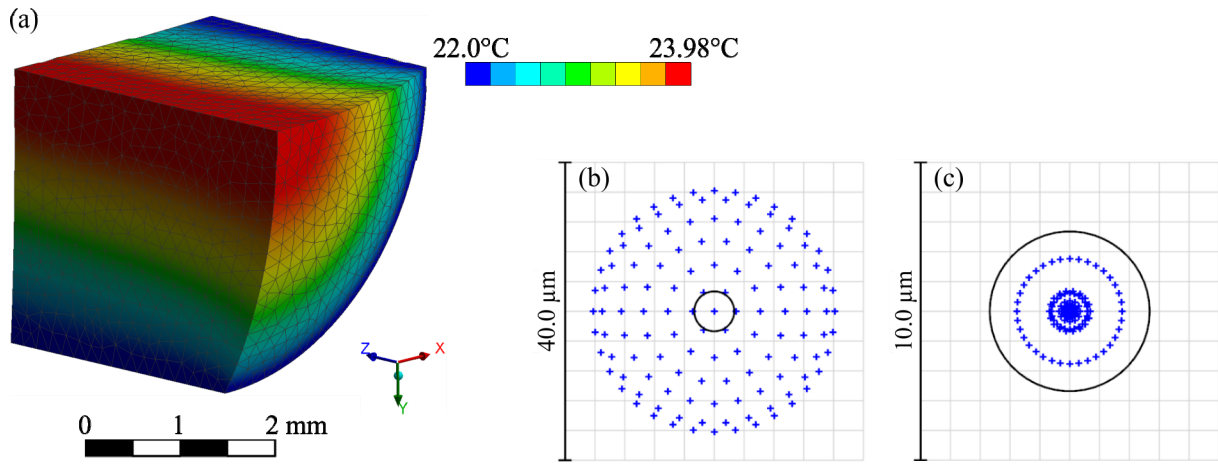

Figure 7. Temperature profile in the bulk of the plastic asphere (a). The spot diagram in the original focal plane (b) and in the new focal plane, which is shifted about +132 µm (c).

4.2 Modeling of the thermal deformation

In a second step, only the thermally induced surface deformation is taken into account. The deformation of the bulk is shown in figure 8(a). The corresponding axial and radial deformation is depicted in figure 9 for the front and back surface. The maximal axial deformation takes place on the optical axis while the maximal radial deformation can be observed at approximately 2/3 of the lens diameter. On the front surface, the radial deformation has a maximum of 0.80 µm and, due to the small curvature radius, clearly contributes to the deformation sag. At a radial positon equal to the beam diameter ($r = 2.0$ mm), the radial deformation constitutes 20% of the deformation sag. This amount is not negligible. In contrast, the maximal radial deformation of 0.41 µm on the back surface has nearly no influence on the deformation sag because the curvature radius is seven times larger. The maximal deformation sag coincides with the maximal axial deformation and is 2.2 µm on the front surface and 1.6 µm on the back surface. These values are approximately a factor of 5 smaller than the typical manufacturing tolerances for injection-molded lenses [18]. However, since the deformation is inhomogeneous over the aperture, it will influence the focal beam intensity distribution.

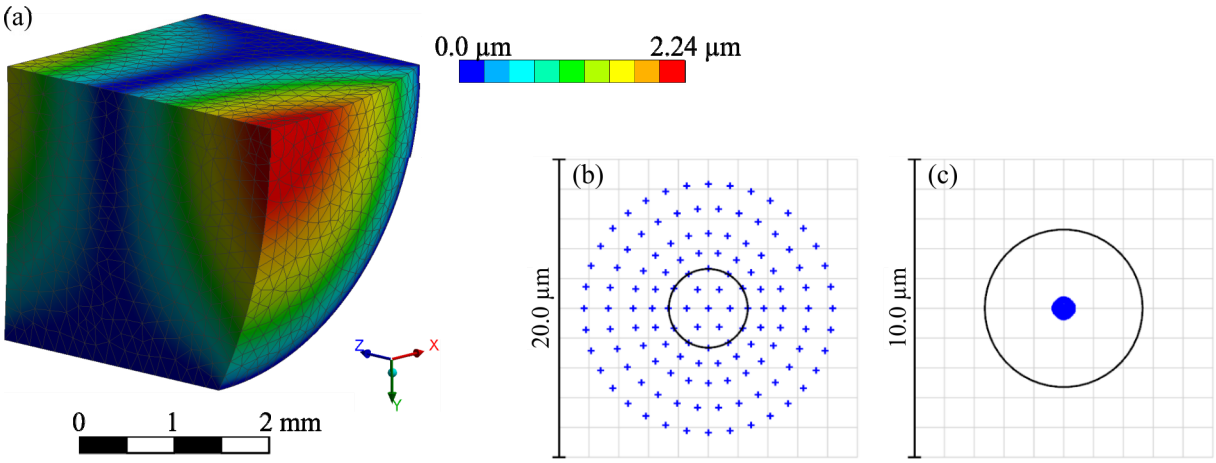

Figure 8. Bulk deformation of the plastic asphere (a). The spot diagram in the original focal plane (b) and in the new focal plane, which is shifted about −59 µm (c).

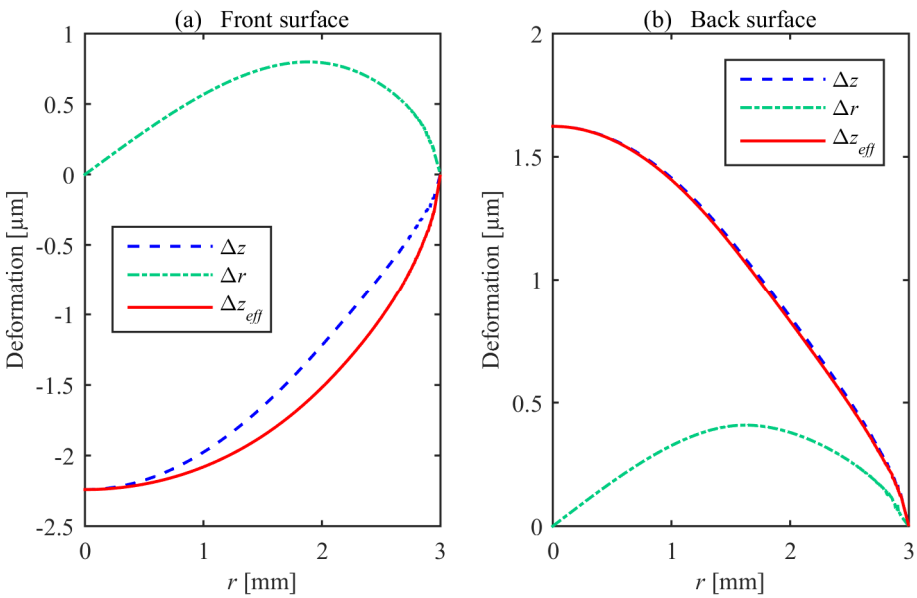

Figure 9. Comparison of axial and radial deformation with the deformation sag: (a) for the front surface and (b) for the back surface. The radial deformation clearly contributes to the deformation sag of the front surface.

The deformation sag of the front surface is approximated with a polynomial of degree 10; a polynomial degree of 8 is used for the back surface. The RMSE of the approximation is 0.01 µm and 0.005 µm, respectively. In the optical analysis, the surface deformation leads to a focal shift of −59 µm. The spot size in the new focal plane is still diffraction limited (cf. figure 8(c) and table 4).

4.3 Effect of self-compensation

Finally, the GRIN profile and the surface deformation are both considered. The resulting spot diagrams in the original and the new focal plane are depicted in figure 10. Furthermore, table 4 shows the focal shift and the RMS spot sizes in the original and the new focal plane. The total focal shift is +73 µm, which equals the sum of the focal shift caused by the GRIN profile and thermal deformation. The RMS spot is 7.1 µm in the original and 1.2 µm in the new focal plane. Although the spot in the new focal plane is diffraction limited, aberrations can be observed as the transverse ray fan in figure 10(c) shows.

The lens material LSR 7070 is partially self-compensating because the focal shift induced by the GRIN profile is reduced by the focal shift due to deformation. In case of a thermo-optical constant with different sign but same amount, the focal shift would have been −188 µm instead of +73 µm.

Table 4. RMS spot size and focal shift for the different analyzed cases. The Airy radius is always 2.7 µm.

	RMS spot size [µm] in original focal plane	**RMS spot size [µm] in new focal plane**	**Focal shift [µm]**
"Cold" system	0.009	-	-
Only GRIN	13.2	1.0	+132
Only deformation	6.2	0.22	−59
GRIN & deformation	7.1	1.2	+73

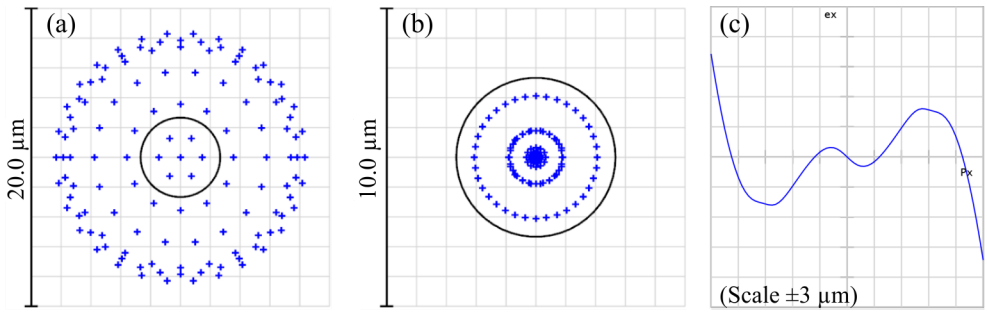

Figure 10. Spot diagram in the original focal plane (a) and in the new focal plane, which is shifted about +73 µm (b). Transverse ray fan in the new focal plane (c).

5. CONCLUSION

Coupled thermo-optical simulation plays an increasing role in optical design. On the one hand, higher available laser powers and the attempt for miniaturization cause a steadily increasing thermal load of optical elements. On the other hand, pricing pressure leads to the increased use of inexpensive plastic lenses, which are suitable for mass production but feature high thermal expansion. Thermo-optical effects influence optical properties and can significantly reduce the system's beam quality.

An approach for modeling thermally induced surface deformations by using a global even polynomial has been demonstrated. The discrete deformation data resulting from a FEA are approximated and transferred to optical ray-tracing. Thereby, the radial surface deformation is taken into account. The implemented algorithm has been verified by an analytic test case. The existing coupling between FEA and ray-tracing, which enables the modeling of the temperature dependent refractive index profile, has been extended by the new surface deformation feature. A first application onto a plastic asphere has been performed and points out that for plastic lenses, the thermal deformation can contribute about 30% to the total focal shift.

Further work requires the extension of the approximation algorithm to non-rotational symmetric surface deformations in order to model more complex optical systems featuring, for example, non-axial radiation or asymmetric cooling conditions. Additionally, an experimental measurement of the focal shift of a lens, preferably made of plastic so that thermal deformation is significant, and its comparison to the simulation are desirable.

ACKNOWLEDGEMENTS

The authors thank the German Research Foundation (DFG) for its support within the project "Experimentelle und theoretische Untersuchungen zu thermisch induzierten Aberrationen optischer Systeme für die Lasermaterialbearbeitung" at RWTH Aachen University.

REFERENCES

[1] Gatej, A., Thombansen, U., and Loosen P., "Kombinierte Thermo-Optische Simulation für Optische Systeme," DGaO Proceedings 112, B021-6 (2011).
[2] Zemax LLC, OpticStudio, http://www.zemax.com/
[3] Open Engineering S.A., OOFELIE::Multiphysics, http://www.open-engineering.com/
[4] Mazzoli, A., Saint-Georges, P., Orban, A., Ruess, J.-S., Loicq, J., Barbier, C., Stockman, Y., Georges, M., Nachtergaele, P., Paquay, S., and De Vincenzo, P., "Experimental validation of opto-thermo-elastic modeling in OOFELIE Multiphysics," Proc. SPIE 8167, 81671I–81671I-15 (2011).
[5] Sigmadyne Inc., SigFit, http://sigmadyne.com/
[6] Michels, G. J., and Genberg, V. L., "Analysis of thermally loaded transmissive optical elements," Proc. SPIE 8840, 88400C–88400C-8 (2013).
[7] Gatej, A., Wasselowski, J., and Loosen, P., "Thermo-optical (TOP) analysis by coupling FEM and ray tracing," Proc. SPIE 8429, 84290E–84290E-8 (2012).
[8] Gatej, A., Richmann, A., Pütsch, O., and Loosen, P., "Thermo-Optical (TOP) analysis of transmissive elements for laser-systems," Proc. SPIE 8490, 84900C–84900C-10 (2012).
[9] Gatej, A., Wasselowski, J., and Loosen, P., "Using adaptive weighted least squares approximation for coupling thermal and optical simulation," Appl. Opt. 51(28), 6718–6725 (2012).
[10] Doyle, K. B., Genberg, V. L., Michels, G. J., and Bisson, G. R., "Optical modeling of finite element surface displacements using commercial software," Proc. SPIE 5867, 58670I–58670I-12 (2005).
[11] Coronato, P. A., and Juergens, R. C., "Transferring FEA results to optics codes with Zernikes: a review of techniques," Proc. SPIE 5176, 1–8 (2003).
[12] Juergens R. C., and Coronato, P. A., "Improved method for transfer of FEA results to optical codes," Proc. of SPIE 5174, 105–115 (2003).
[13] Ansys Inc., Ansys 16.1, http://www.ansys.com/
[14] Schott, "Optical Glass Data Sheets," http://www.schott.com/advanced_optics/english/products/optical-materials/optical-glass/optical-glass/index.html. (25 April 2013).
[15] Momentive Performance Materials Inc., Datasheet "Durable Versatile Optically Clear – Ultra Clear Liquid Silicone Rubber Silopren* LSR 7000 Series" (2013).
[16] Pontes, A., and Bayerl, H., "Silicone Elastomers – Clear as Glass," SAE Technical Paper, 2012-36-0446 (2012).
[17] Franssen, O., and Bayerl, H., "Winning against functional competition – The success story of silicones," Rubber, Fibres and Plastics 7, 156–160 (2012).
[18] Bäumer, S. (Ed.), [Handbook of plastic optics], Wiley-VCH, Weinheim, chapter 2.5.2 (2010).